STEREO VISION-BASED 3D CAMERA POSE AND OBJECT STRUCTURE ESTIMATION
An Application to Service Robotics

Sorin M. Grigorescu, Tiberiu T. Cociaş, Gigel Maceşanu and Florin Moldoveanu
Department of Automation, Transilvania University of Braşov, Mihai Viteazu 5, 500174, Braşov, Romania

Keywords: Robot Vision, 3D Reconstruction, Stereo Vision, Volumetric Object Modeling.

Abstract: In this paper, a robotic pose (position and orientation) estimation and volumetric object modeling system is proposed. The main goal of the methods is to reliably detect the structure of objects of interest present in a visualized robotic scene, together with a precise estimation of the robot's pose with respect to the detected objects. The robustness of the robotic pose estimation module is achieved by filtering the 2D correspondence matches in order to detect false positives. Once the pose of the robot is obtained, the volumetric structure of the imaged objects of interest is reconstructed through 3D shape primitives and a 3D Region of Interest (ROI).

1 INTRODUCTION

In 3D robotic scene perception, there are usually two types of vision sensors used for acquiring visual information, that is, *stereo vision cameras* and *range sensors* such as laser scanners or 3D *Time-of-Flight* (ToF) cameras (Hussmann and Liepert, 2007). In the process of stereo vision based 3D perception and ego-motion estimation, the stereo correspondence problem has to be solved, i.e. the corresponding feature points, necessary for 3D reconstruction, have to be extracted from both stereo images (Brown et al., 2003). In contrast, stereo vision range sensing devices provide direct capturing of 3D scenes, delivering a pure stereo depth image in form of 3D point clouds. In the case of range sensors, the obtained depth information can have different error values, depending on the sensed surface. This phenomenon makes stereo vision a more reliable solution for autonomous robotic systems that operate in real world environments.

Camera pose estimation has been studied within the *Simultaneous Localization and Mapping* (SLAM) context. Using detected visual information, motion estimation techniques can provide a very precise ego-motion of the robot. The main operation involved in stereo based robotic perception is the computation of the so-called *correspondence points* used for calculating the 3D pose of the robot's camera (Geiger et al., 2011). The most common features used in this context are points localized through corner detectors such as *Harris*. Based on the extracted features, the robot's motion can be extracted with the help of estimators such as the *Kalman* or *Particle Filter*.

In the last years, the 3D reconstruction and modeling of objects has become a topic of interest for several fields of research such as robotics, virtual reality, medicine, surveillance and industry (Davies et al., 2008). The main contributions of the presented paper may be summarized as follows:

1. camera pose and 3D scene structure estimation pipeline for on-line scene understanding;
2. automatic calculation of a 3D ROI for initializing the 3D object volumetric estimation algorithm;
3. object grasping points calculation via 3D volumetric modeling from generic shape primitives in highly noisy data (e.g. disparity images).

2 CAMERA POSE ESTIMATION

The block diagram of the proposed vision system is presented in Fig. 1. The sequence of stereo images is organized into so-called tracks which include key features from the imaged scene and geometric constraints which are used to solve the pose estimation problem. One of these elements are the matched 2D feature points between the left and the right images of the stereo camera. The accuracy of pose estimation is directly dependent on the precision of 2D correspondence matching. In order to filter out bad matches,

M. Grigorescu S., T. CociaÈŹ T., MaceÈŹanu G. and Moldoveanu F..
STEREO VISION-BASED 3D CAMERA POSE AND OBJECT STRUCTURE ESTIMATION - An Application to Service Robotics.
DOI: 10.5220/0003819403550358
In *Proceedings of the International Conference on Computer Vision Theory and Applications* (VISAPP-2012), pages 355-358
ISBN: 978-989-8565-04-4

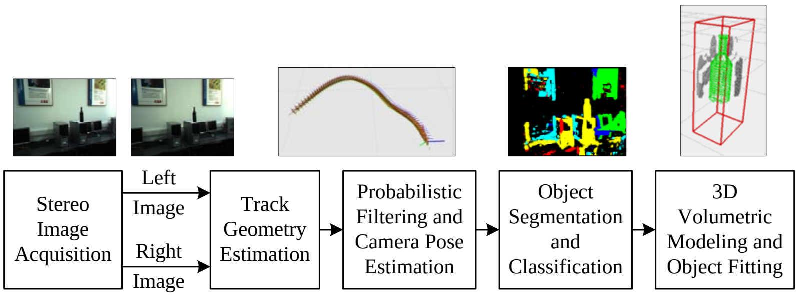
Stereo Image Acquisition
Left Image
Right Image
Track Geometry Estimation
Probabilistic Filtering and Camera Pose Estimation
Object Segmentation and Classification
3D Volumetric Modeling and Object Fitting

Figure 1: Block diagram of the proposed camera pose estimation and object volumetric modeling architecture.

a probabilistic filtering approach, which exploits the geometrical constraints of the stereo camera, is proposed.

2D feature points have been extracted via the Harris corner detector, followed by a correspondence matching using a traditional cross-correlation similarity measure. Secondly, a matching is performed between the 2D feature points in consecutive stereo images, that is, between images acquired under camera poses $C(k)$ and $C(k+1)$. As convention, these matches are calculated for the left camera only. Knowing the 3D positions of the 2D points matched between adjacent images, the pose of the camera can be calculated through a *Perspective-N-Point* (PNP) algorithm (Hartley and Zisserman, 2004).

The obtained pose is further refined using a Kalman filter. Once the camera pose estimation problem has been solved, the 3D relation between the robot and the imaged objects of interest has to be calculated, that is, the establishment of the 3D positions of the objects grasping points. This process is divided into two stages. An initial raw object localization is obtained through a depth image segmentation and object classification. Further, the detection of the 3D grasping points is calculated by statistically fitting a shape primitive, based on the object classification information. One of the main contributions of the paper is actually the calculation of an object's grasping points through a shape primitive. As it will be explained, the primitive is independent of a particular object shape, its fitting being guided by so-called *primitive control points*. In other words, a shape can be fitted to a broad range of objects belonging to that specific class.

The process of matching stereo features is usually corrupted by noise and delivers false matches along with the true correspondences. In order to overcome this problem, we have chosen to filter out the bad matches by exploiting the geometrical relations within a stereo camera. Namely, we take into account that the majority of the points are true positive. Hence, we can approximate the probability density of the real matches by calculating the slope of the line connecting the correspondences in two images:

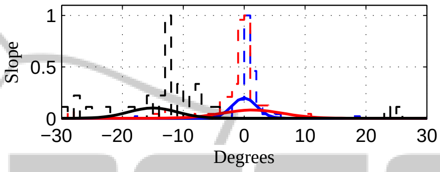

Figure 2: Slope filtering models.

$$m = \frac{p_{R_y} - p_{L_y}}{p_{R_x} - p_{L_x}}, \; m \in \mathbf{M}, \tag{1}$$

where m is the slope between the left and right image points $p_L(x,y)$ and $p_R(x,y)$, respectively. Taking into account a Gaussian probability distribution of the slope, a *Maximum Likelihood Estimator* (MLE) has been used for calculating the parameters of the model, that is the mean θ_μ and variance θ_σ:

$$\widehat{\theta} = \arg\max_{\theta \in \Theta} L(\theta|\mathbf{M}), \tag{2}$$

where $\widehat{\theta}$ is the obtained maximum likelihood estimate for the Gaussian *Probability Distribution Function* (PDF) $p(\mathbf{M}|\theta_\mu, \theta_\sigma)$ describing the distribution of the lines slope. In Fig. 2, three examples of slope PDF estimation can be seen. Using the obtained model, the feature points can be classified into inliers and outliers, as in the classical RANSAC approach.

Once a certain camera pose has been calculated, it is filtered out using a standard Kalman filter with a state vector defined as the measured rotation and translation of the sensor $\mathbf{x} = \begin{bmatrix} x_i & y_i & z_i & \phi_i & \psi_i & \theta_i \end{bmatrix}^T$. The transition matrix F of the Kalman update equation $\mathbf{x}(k+1) = \mathbf{F} \cdot \mathbf{x}(k) + w(k)$ encodes a constant camera velocity, with zero acceleration. One major problem that has to be solved in depth map fusion is the redundant information coming from overlapping projected disparity images. In order to save computation time, we have considered as valid voxels those ones visible in the newest images acquired from the stereo camera. An example

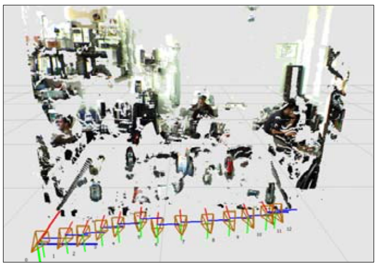

Figure 3: Annotated 3D model from depth maps fusion.

of depth maps fusion within a robotic scene is given in Fig. 3.

3 3D OBJECT VOLUMETRIC MODELING

In order to fit a shape primitive over the depth information, the imaged objects have to be segmented and classified. The feature vector used for this operation is composed of the camera-object distance, described by the disparity map, and the color distribution of the objects represented in the HSV (*Hue*, *Value*, *Saturation*) color space. The segmentation result classifies image pixels into object classes, as seen in Fig. 1. The 2D segmentation information will be further used for defining a 3D ROI, which actually initializes the shape fitting algorithm. This is the starting point used for deforming the shape primitive in order to fit the segmented object.

An object ROI is defined in a stereo image pair as the feature vector $[p_{L_i}, p_{R_i}]$, $i = 1,2,3,4$, containing the four corresponding 2D points in the left and right images. Knowing the geometry of the stereo camera, the ROI vector can be reprojected into a virtual 3D environment by calculating the disparity between p_{L_i} and p_{R_i} (Brown et al., 2003). The volumetric properties of the ROI, namely its 3D volume, are calculated from the reprojected depth map, that is, from the 3D distribution of the disparity points calculated using the robust Block Matching approach from (Grigorescu and Moldoveanu, 2011). The center of the ROI over the Z axis is given by the highest disparity points density obtained as a maximization over the disparity value. The front and back positions of the ROI are given by the nearest and farthest values in the disparity. An example of a 3D ROI can be seen in Fig. 4.

A shape primitive is represented as a *Point Distribution Model* (PDM) containing a vector of 3D locations S related to a common reference coordinate system:

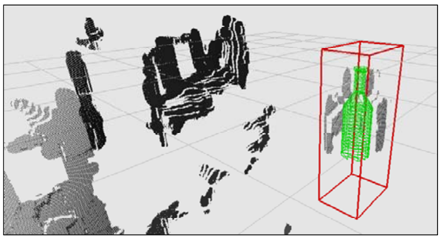

Figure 4: Reprojected 3D ROI and PDM mesh primitive.

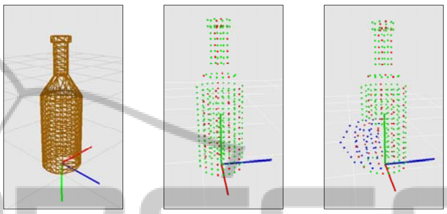

(a) (b) (c)

Figure 5: Object shape primitive fitting example. (a) Shape primitive. (b) PDM model with control points marked with red. (c) Deformed shape using a control point (affected points marked with blue).

$$x^{(i)} \in S, \; i = 1,2,...,n_p, \tag{3}$$

where x is a point on the primitive shape and n_p the total number of primitive points. A mesh PDM example can be seen in Fig. 5(a). The 3D ROI is used to position the shape on the center of gravity of the ROI. Once it is centered, its rotation, translation and scaling is modified through a similarity transform:

$$\mathbf{X}_{new} = sR(\mathbf{X}_{old} + T), \tag{4}$$

where $\mathbf{X}_{old}$ and $\mathbf{X}_{new}$ are the old and new 3D positions of the primitive shape points, R and t are rotation and translation matrices, respectively, and s represents a scaling factor.

The last step in the proposed vision system is the fitting of the object's primitive on the disparity information. This procedure is performed using a set of socalled *control points* which regulate the structure of the shape. Such control points have been introduced in medical imaging for modeling deformable shapes such as the hearth (Zheng et al., 2008). To the best of our knowledge, this is the first application of control points fitting a shape primitive in a stereo-vision based system used in visual guided object grasping. In the PDM from Fig. 5(b), the control points are represented as the red locations. In the example from Fig. 5(c), the shape is deformed by changing the location of one control point. Following a simple linear transformation, the neighboring points are automatically translated with respect to the new position of the control point.

In order to drive the control points to their optimal 3D locations, a relation between the disparity information contained within the ROI and the control points on the shape primitive had to be derived. This is accomplished by estimating the surface normal of the disparity areas with respect to the control points, that is, each control points if moved in the direction of the nearest disparity surface according to its normal.

The advantage of modeling the complete 3D shape of the objects for grasping purposes plays a crucial role in the grasping procedure. Namely, if each object 3D point is precisely related to the pose of the robotic system, obtained through the algorithm from Section 2, then the control precision of autonomous robots equipped with redundant manipulators is much higher than for the case when object grasping points are directly extracted from 2D visual information.

Table 1: Statistical position and orienation errors allong the three Cartesian axes between the proposed and marker based 3D camera pose estimation.

	X_e [m; deg]	Y_e [m; deg]	Z_e [m; deg]
Max err.	0.049; 4.2	0.059; 5.6	0.101; 10.1
Mean	0.013; 0.7	0.014; 0.7	0.042; 0.6
Std. dev.	0.021; 2.3	0.02; 2.6	0.064; 5.5

4 PERFORMANCE EVALUATION

The evaluation of the proposed machine vision system has been performed with respect to the real 3D poses of the objects of interest. The real 3D positions and orientations of the objects of interest were manually determined using the following setup. On the imaged scene, a visual marker, considered to be the *ground truth* information, was installed in such a way that the poses of the objects could be easily measured with respect to the marker. The 3D pose of the marker was detected using the ARToolKit library which provides subpixel accuracy estimation of the marker's location with an average error of $\approx 5mm$. By calculating the marker's 3D pose, a ground truth reference value for camera position and orientation estimation could be obtained using the inverse of the marker's pose matrix. Further, the positions of the camera poses were calculated using the proposed system. The results were compared to the ground truth data provided by the ARToolKit marker.

The marker-less pose estimation algorithm described in this paper delivered a camera position and orientation closely related to the ground truth values. This correlation can be easily observed when analysing the statistical error results, given in Tab. 1, between the two approaches. Namely, for both the position and orientation, the errors are small enough to ensure a good spatial localization of the camera, or robot, and also to provide reliable depth maps fusion.

5 CONCLUSIONS

In this paper a camera pose and 3D object volumetric system for service robotics purposes has been proposed. Its goal is to precisely determine the 3D structure of the imaged objects of interest with respect to the pose of the camera, that is, of the robot itself. As future work, the authors consider the speed enhancement of the proposed system using state of the art parallel processing equipment.

ACKNOWLEDGEMENTS

This paper is supported by the Sectoral Operational Program Human Resources Development (SOP HRD), financed from the European Social Fund and by the Romanian Government under the projects POSDRU/89/1.5/S/59323 and POSDRU/107/1.5/S/76945.

REFERENCES

Brown, M., Burschka, D., and Hager, G. (2003). Advances in Computational Stereo. *IEEE Trans. on Pattern Recognition and Machine Intelligence*, 25(8):993–1008.

Davies, R., Twining, C., and Taylor, C. (2008). *Statistical Models of Shape: Optimisation and Evaluation*. Springer.

Geiger, A., Ziegler, J., and Stiller, C. (2011). StereoScan: Dense 3D Reconstruction in Real-time. In *IEEE Intelligent Vehicles Symposium*, Baden-Baden, Germany.

Grigorescu, S. and Moldoveanu, F. (2011). Controlling Depth Estimation for Robust Robotic Perception. In *Proc. of the 18th IFAC World Congress*, Milano, Italy.

Hartley, R. and Zisserman, A. (2004). *Multiple View Geometry in Computer Vision*. Cambridge University Press.

Hussmann, S. and Liepert, T. (2007). Robot Vision System based on a 3D-TOF Camera. In *Instrumentation and Measurement Technology Conference-IMTC 2007*, Warsaw, Poland.

Zheng, Y., Barbu, A., Georgescu, B., Scheuering, M., and Comaniciu, D. (2008). Four-Chamber Heart Modeling and Automatic Segmentation for 3D Cardiac CT Volumes Using Marginal Space Learning and Steerable Features. *IEEE Trans. on Medical Imaging*, 27(11):1668–1681.